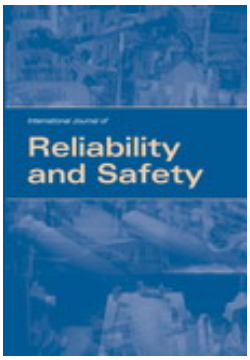


**International Journal of Reliability and Safety**

ISSN online: 1479-3903 - ISSN print: 1479-389X
https://www.inderscience.com/ijrs

# Blast resistance prediction of clay brick masonry wall strengthened with steel wire mesh, and C-FRP laminate under explosion loading: a finite element analysis

Mohd Shariq, S.M. Anas, Mehtab Alam

**DOI:** 10.1504/IJRS.2022.10051370

**Article History:**

| | |
|---|---|
| Received: | 08 August 2022 |
| Accepted: | 23 August 2022 |
| Published online: | 30 January 2023 |

# Blast resistance prediction of clay brick masonry wall strengthened with steel wire mesh, and C-FRP laminate under explosion loading: a finite element analysis

Mohd Shariq* and S.M. Anas

Department of Civil Engineering,
Faculty of Engineering and Technology,
Jamia Millia Islamia (A Central University),
New Delhi, India
Email: shariqqq786@gmail.com
Email: mohdanas43@gmail.com
*Corresponding author

Mehtab Alam

Department of Civil Engineering,
Netaji Subhas University of Technology (West Campus),
New Delhi, India
Email: mehtab.alam@nsut.ac.in

**Abstract:** A detailed finite element micro-model of an Unreinforced Masonry (URM) wall of clay bricks, 1600 mm × 2100 mm × 240 mm, is made in ABAQUS/Explicit-v.6.15 code and analysed considering strain rate effects under the 5 kg-TNT explosion load at 0.58 m/kg$^{1/3}$ scaled distance in free air. Results are validated with the available blast test results. Strengthening of the wall is considered by providing (1) steel wire mesh of diameter 2.50, 3.50 and 4.50 mm on the (a) rear face only and (b) on both the faces; (2) C-FRP wrapping of a thickness (a) 0.50 mm (b) 0.60 mm on the rear face only and (c) 0.30 mm on both the faces of the wall. Response of wall with each strengthening technique applied in this study is discussed. Application of 4.50 mm wire mesh on both the faces and 0.50 mm C-FRP sheet on the rear face makes the wall respond with comparable performance under the considered blast loading.

**Keywords:** explosion loading; masonry walls; building safety; clay bricks; steel mesh; C-FRP wrapping; blast resistance; damage.

**Reference** to this paper should be made as follows: Shariq, M., Anas, S.M. and Alam, M. (2022) 'Blast resistance prediction of clay brick masonry wall strengthened with steel wire mesh, and C-FRP laminate under explosion loading: a finite element analysis', *Int. J. Reliability and Safety*, Vol. 16, Nos. 1/2, pp.27–45.

**Biographical notes:** Mohd Shariq is currently working as a PhD Scholar in the Department of Civil Engineering, Faculty of Engineering and Technology, Jamia Millia Islamia, New Delhi, India. He received his Bachelor of Technology (Civil) and a Master of Technology (Earthquake Eng.) with Honours. He is a Civil Engineer with great experience in structural analysis,

blast simulation and finite element modelling. Their current project is 'blast analysis of masonry compression members'.

S.M. Anas is a PhD scholar in the Department of Civil Engineering within the Faculty of Engineering and Technology, Jamia Millia Islamia (A Central University), Jamia Nagar, New Delhi, India. He received his Bachelor of Technology (Civil) degree from Sharda University and a Master of Technology (Earthquake Eng.) degree with honours from Jamia Millia Islamia. His research interests include strengthening techniques, finite element modelling, structural performance, composite materials, FRP, AFRP, BFRP, C-FRP, GFRP, steel tubes, metallic foams, pre-tensioned concrete girders, blast-resistant shelters, heritage masonry buildings, masonry walls, underground blasting, ground shock, impact-resistant structures, impulsive-loadings, among others.

Mehtab Alam is currently Professor Emeritus in the Civil Engineering Department, Netaji Subhas University of Technology, West Campus, New Delhi, India. He is a Member of Several Societies such as the Indian Society of Earthquake Technology (IIT-Roorkee), the Indian Society of Technical Education, the Ferro Cement Society of India and so on. His teaching and research interests include structural behaviour and design, structural mechanics, construction materials, recycling of demolished concrete waste, skin-reinforced concrete, earthquake disaster and crisis-management with emphasis on RC slab systems, FRP concrete materials and their structural applications, structural safety and design code development.

## 1 Introduction

Unreinforced masonry constructions have negative consequences from impulsive loadings, which reduces their ability to handle axial loads. Masonry building is a traditional method that has been utilised to build infrastructure for economically disadvantaged groups in rural areas for a very long time (Anas et al., 2021c; Pandey and Bisht, 2014; Ahmadi et al., 2021; Anas et al., 2020a, 2020b, 2020c; Anas et al., 2021a, 2021b; Anas and Alam, 2021a, 2021b; Anas et al., 2021c, 2021d, 2021e, 2021f; Anas and Alam, 2022a, 2022b, 2022c; Anas et al., 2022a, 2022b, 2022c, 2022d, 2022e, 2022f, 2022g, 2022h, 2022i, 2022j, 2022k; Ahmadi et al., 2022; Shariq et al., 2022a; 2022b, 2022c, 2022d; Tahzeeb et al., 2022a, 2022b, 2022c; UlAin et al., 2021, 2022; Milani and Lourenco, 2009; Milani et al., 2009; Aamir et al., 2022; Anas et al., 2021g). Unreinforced masonry has a weak resistance to out-of-plane stress due to its brittle nature (Ehsani and Pena, 2009). At least one of the three prevalent forms of failures, namely tensile failure, compression failure in zones of severe flexure and shear failure close to the support, are often present in masonry walls exposed to explosions (Myers et al., 2004). For academics and engineers, the safety issue with masonry walls subjected to blast loading is a problem and a research area. The first technique is the traditional retrofitting procedure, in which steel and concrete are added to these walls to boost their strength (Anas et al., 2021c, 2021e, Badshah et al., 2021). The disadvantage of this approach is that it requires more time and money. However, employing C-FRP and other materials that are openly available in the literature, researchers have created and

recognised new strengthening methods to improve the blast enhancement of masonry buildings (Shamim et al., 2019; Anas and Alam, 2022a, 2022b, 2022c; Anas et al., 2022a, 2022b, 2022c, 2022d, 2022e, 2022f, 2022g, 2022h, 2022i, 2022j, 2022k; Ahmadi et al., 2022; Shariq et al., 2022a; 2022b, 2022c, 2022d; Tahzeeb et al., 2022a, 2022b, 2022c; UlAin et al., 2021, 2022; Milani and Lourenco, 2009; Milani et al., 2009; Aamir et al., 2022; Anas et al., 2021g).

## 2 Past studies

A 100 kg TNT surface burst was studied by Pandey and Bisht (2014) at stand-off distances of 20 m, 30 m and 40 m. Three grades of concrete mortar – 1:6, 1:4.5 and 1:3 – were investigated in the study on walls that were 340 and 235 millimetres thick and were in filled in RC frames. The RC frame's cross-section was 350 mm × 345 mm while the walls' length and height were also 3000 mm. A further 13.46 MPa was the total strength of the brick, while 6.78 MPa, 13.86 MPa and 24.80 MPa, respectively, were the strengths of the three grade mortars (1:6, 1:4.5 and 1:3). The RC frame's steel and concrete grades were M15 and Fe415, respectively. The study's findings showed that a 340mm thick masonry wall had become unusable after blasting for three different classes of masonry at a blast force of 100 kg TNT at a 20m detonation distance. Additionally, for all mortar grades that indicated re-usable masonry, the deflection was relatively lower for the case of a 40 m detonation distance. Two Un-Retrofitted Masonry (URM) walls measuring 11 feet tall, 8 feet long and 8 inches thick were created by Ehsani and Pena (2009) using conventional mortar mixture and 16×8×8-inch masonry blocks. The masonry's compressive strength was 1500 psi (10.34 MPa). C-FRP was adapted onto one URM wall on both sides. With a 30-foot standoff, a 200 pound (90.8 Kg) TNT charge was detonated in front of the walls. According to the study's findings, an efficient application of C-FRP retrofitting prevented the collapse of the URM wall and kept all of the masonry rubble inside the C-FRP. Wu et al. (2021) experimental investigation used 8 clay brick masonry walls that were each 2.1 × 1.6 × 0.24 m in size. The bricks used in the masonry walls have dimensions of 240 mm × 115 mm × 53 mm and a compressive strength of 15.5 MPa. The mortar used in the construction had a 10 mm thickness and was estimated to have an average compressive strength of 4.9 MPa. On both sides of the wall, 10 mm of plaster was first laid, then a 3 mm layer of polyurea. A 5 kg TNT blast load was applied to the wall at three different standoff distances: 1.5 m, 1 m and 0.6 m. The study found that applying a polyurea coating considerably increased the walls' ability to withstand blasts, with the effect being greater on the back face of the walls than the front.

A brick-wall with dimensions of 2656 mm in height and 3590 mm in length was given a numerical analysis by Wei and Stewart (2010), and its thickness was divided into 3 separate ranges: 110 mm, 230 mm and 350 mm. The bricks used to construct the wall were 230 mm by 110 mm by 76 mm in size. Additionally, 3 different grades of mortars (B40, B30 and B20) and 3 different grades of bricks (B40, B30 and B20) were utilised (M5, M10 and M15). 10 mm was the mortar's thickness. A 125 kg TNT explosion charge was employed at varied stand-off distances of 20 m, 25 m, and 30 m to measure the blast reaction of the wall. The investigation came to the conclusion that the structural response to large-scale blast loads was unaffected by the mortar strength and brick strength. Wei et al. (2021) investigation of a brick masonry wall of 1250 mm by 1490 mm by 240 mm employed bricks with dimensions of 240 mm by 115 mm by

53 mm. The mortar was 10 mm thick, and the brick had a compressive strength of 2.6 MPa. The mortar material's primary tensile stress at failure was estimated to be 1 MPa. The explosive charge used in the study was a C4 spherical charge, which had radii of 42.10 mm, 53.04 mm, 66.82 mm and 84.19 mm and was evaluated at varied magnitudes of 0.5 kg, 1 kg, 2 kg and 4 kg. To cause these explosives to detonate, they were placed in the centre of the brick masonry wall's front surface. The experiment came to the conclusion that a circular crater is created when a contact explosion caused by a spherical explosive charge emerges on a brick masonry wall, and its cross-sectional dimensions repeatedly grow as the radius increases. Myers et al. (2004) evaluated the blast response of two different types of brick walls, measuring 2.24 m in height and 1.22 m in length, with thicknesses of 102 mm and 203 mm. Two core hollow concrete blocks with nominal dimensions of 102 mm × 203 mm × 305 mm and 203 mm × 203 mm × 406 mm were used to build the walls. These two hollow concrete blocks have compressive strengths of 10.34 MPa and 12.48 MPa, respectively. Mortar had an average compressive strength of 10.34 MPa. Three alternative methods of wall reinforcement were used during the trial. In the first method, 6.4mm GFRP rods were used at each horizontal junction to reinforce the wall. In the second, three 64 mm wide GFRP strips were used to support the wall vertically. In the final method, GFRP rods and GFRP strips were both used to reinforce the wall. 2.3 kg of PETN blast charge was administered at various stand-off distances ranging from 0.91 to 3.66 m in order to study the explosion reaction. According to the study's findings, FRP composites gave significant advantages in strengthening masonry walls to withstand blast loads.

Unreinforced, ferro-cement overlay and restricted masonry, all measuring 23 mm thick, were the subject of an experimental investigation started by Badshah et al. (2021). The wall was 1.83 m high at this location. Bricks used in construction had dimensions of 23 × 11.40 × 7.60 cm, and masonry had a 3.13 MPa compressive strength. The ferro-cement overlay masonry wall received a coating of ferro-cement that was 19 mm thick. A constrained masonry wall was also reinforced longitudinally with 4 bars of 12 mm each, and transversely with 8 mm stirrups spaced at 150 mm intervals. In the investigation, an expanding range of TNT equivalent charges were employed for the explosion, weighing anywhere between 0.56 kg and 17.8 kg, with a constant stand-off distance of 3.58 m. The experiment demonstrated that the danger of possible human fatalities and material losses was higher in the upper layers of a free-standing masonry wall constructed of ferro-cement overlay masonry and unreinforced bricks. Therefore, in unreinforced boundary masonry walls, precise strengthening procedures such as pre-compression should be applied to the top layers of the brick. A 3000 mm × 230 mm masonry in filled wall was the subject of an investigation by Shamim et al. (2019). The RCC frame's cross-section, which was taken into account for modelling, was 230 mm × 235 mm. In addition, the wall contained a 1000 × 1000 mm hole. A 100 kg TNT charge was used to blast the wall from different standoff distances of 20 m, 30 m and 40 m. The results of the experiment showed that the peak displacement in the masonry walls with and without opening rose with decreasing stand-off distances, indicating that the blast's influence decreased with growing stand-off distances.

## 3 Goals of the current study

The goals of this research are:

- To analyse how the unreinforced masonry-wall responds dynamically to blast loads.
- To look at how C-FRP sheet and steel wire mesh affect how the wall responds to blasts.

## 4 ABAQUS modelling of masonry wall subjected to blast

In order to analyse the blast reaction of the clay brick masonry wall, which has dimensions of 2100 mm (height) × 1600mm (length) × 240mm, ABAQUS/CAE 2019 is being used (thickness). The brick's dimensions are as follows: 240 mm (length), 115 mm (width) and 53 mm (thickness) (Wu et al., 2021). The brick has the following parameters: 15.5 MPa in compressive strength, 1800 kg/m$^3$ in density, 8200 MPa Young's modulus, 0.775 MPa in tensile strength and 0.16 in poison ratio. These brick values were obtained from a research by Wu et al. (2001). On both faces of the brick masonry wall, a 10 mm thick coating of mortar is present. Other mortar characteristics have been extracted from Wu et al. (2021). Ten finite element models in all have been created for this investigation. The first finite element model (US) represents a conventionally un-strengthened wall, and the second, third and fourth models are S-2.5-SWM-R, S-3.5-SWM-R and S-4.5-SWM-R, respectively, where the first English letter "S" stands for a strengthened wall, the second number indicates the diameter of the welded Steel Wire Mesh (SWM), and the final letter "R" indicates that the mesh is only applied to the wall' By adding more wire mesh to the front face of the first three models, the fifth, sixth and seventh models – abbreviated S-2.5-SWM-B, S-3.5-SWM-B, and S-4.5-SWM-B – were created. The final "B" stands for both faces. S-0.5-C-FRP-R and S-0.6-C-FRP-R, the eighth and ninth versions, use 0.50 and 0.60 mm C-FRP sheets laminated to the wall's back face to reinforce the wall. Last but not least, the strengthening of the wall's front and rear faces (i.e., S-0.3-C-FRP-B) has been accomplished utilising a 0.30 mm thick sheet of C-FRP. From Phan-Vu et al. (2021), the characteristics of C-FRP were extracted. For the welded steel wire mesh employed in the investigation, the mass density, yield strength, Young's modulus and Poisson's ratio were calculated as follows: 7850 kg/m$^3$, 250 MPa, 210 GPa and 0.3. In line with IS-4948 (2002), the welded steel wire mesh used in the aforementioned models has a 75 mm centre-to-centre spacing. An amount of 5 kg of TNT was employed as the explosion charge in the investigation, and the stand-off distance was scaled to be 1.0 m (0.584 m/kg$^{1/3}$). The plaster is embedded with wire mesh using the embedded region constraint. To attach the wire mesh to the wall surface, use the tie constraint command. In Wu et al. (2021), experimental test software includes a wall model that takes into account the boundary conditions and other factors.

### *4.1 Explosion loading*

The explosion is a catastrophic wave of highly compressed air or energy that spreads outward, causing a violent crushing of volume. The emission of hot, heavy, high-pressure gases at high temperatures often initiates this process (Ahmadi et al., 2021; Anas et al., 2020a, 2020b, 2020c; Anas et al., 2021a, 2021b; Anas and Alam, 2021a, 2021b; Anas

et al., 2021c, 2021d, 2021e, 2021f; Anas and Alam, 2022a, 2022b, 2022c; Anas et al., 2022a, 2022b, 2022c, 2022d, 2022e, 2022f, 2022g, 2022h, 2022i, 2022j, 2022k; Ahmadi et al., 2022; Shariq et al., 2022a; 2022b, 2022c, 2022d; Tahzeeb et al., 2022a, 2022b, 2022c; UlAin et al., 2021, 2022). A strong oxidation process that results in an explosion triggered by a blast releases a significant amount of energy in the form of light, heat, and sound for a brief yet devastating period of time. The blast pressure profile is illustrated in Figure 1 and starts with a value of atmospheric pressure (Anas and Alam, 2021a; Anas et al., 2021d; Goel and Matsagar, 2014; Hao et al., 2016; Wu and Hao, 2005; Anas and Alam, 2022a, 2022b, 2022c; Anas et al., 2022a, 2022b, 2022c, 2022d, 2022e, 2022f, 2022g, 2022h, 2022i, 2022j, 2022k; Ahmadi et al., 2022; Shariq et al., 2022a; 2022b, 2022c, 2022d; Tahzeeb et al., 2022a, 2022b, 2022c; UlAin et al., 2021, 2022. The symbol $t_A$ indicates how long it took the blast wave to get to the area of interest (Time of arrival). The explosion takes place at time $t_A$, leading to an instantaneous rise in pressure, which is shown by $P_i$ (peak over-pressure), for a very brief period of time. The $P_i$ (Peak over-pressure) is extremely important to employ on the blast face since it has the biggest magnitude during the entire blast event. The term $t_d$ in the equation stands for the amount of time that the pressure has been greater than the atmospheric pressure (Anas et al., 2020a, 2020c, 2021b; Hao et al., 2016). After a brief period of time, the pressure of time begins to fall down exponentially, bringing the values of pressure and atmospheric pressure to a point where they are equal. As the value of pressure steadily decreases and eventually equals the value of atmospheric pressure, the vacuum is created and the pressure goes negative (Ahmadi et al., 2021; Anas et al., 2021f; Goel and Matsagar, 2014; Wu and Hao, 2005). Negative phase duration is the amount of time that the pressure has been lower than the atmospheric pressure. The theory of the time history of air blast wave pressure of the blast mechanism was clarified by Wu and Hao (2005), who also offered an empirical method to determine the values of air blast wave variables such as arrival time, rising time and positive phase length.

$$t_A = 0.34 S^{1.4} W^{-0.2} / C_a \tag{1}$$

Here, $W$ = Explosive charge (kg); $S$ = Detonation distance (m); $C_a$ = Speed of sound in air = 340 m/sec; $t_A$ = Arrival time of blast wave (sec)

$$t_1 = 0.0019\left(\frac{s}{w^{0.33}}\right)^{1.30} \tag{2}$$

$$t_2 = 0.0005 S^{0.72} W^{0.16} \tag{3}$$

$$t_d = t_1 + t_2 \tag{4}$$

$$P(t) = \left\{ \begin{array}{cc} P_a & (0 \le t < t_A) \\ P_a + P_i\left(\frac{t}{t_i}\right) & (t_A \le t \le t_1) \\ P_a + P_i\left(1 - \frac{t - t_1}{t_2}\right).exp\left(-\frac{\xi(t - t_1)}{t_2}\right) & (t_1 \le t) \end{array} \right\} \tag{5}$$

Here, $t_1$ = Rising time (sec); $t_d$ = duration of positive phase (sec); $t_2$ = Decreasing time (sec); $P_a$ = atmospheric pressure = 0.1MPa; $P_i$ = Peak overpressure (MPa); $\xi$ = decay coefficient.

$$\xi = \begin{Bmatrix} 3.02P_i^{0.38} + 6.85P_i^{0.79}.exp\left(-4.55\dfrac{t-t_1}{t_2}\right) & \left(t_1 \le t \le t_d\right) \\ 1.96P_i^{0.25} + 0.176P_i.exp\left(-0.73P_i^{-0.49}.\left(\dfrac{t-t_d}{t_2}\right)\right) & \left(t_d < t\right) \end{Bmatrix} \quad (6)$$

For $P_i \le 1.0$; And,

$$\xi = \begin{Bmatrix} 1.62P_i^{0.30} + 5.13P_i^{0.28}.exp\left(-1.05P^{0.37}.\left(\dfrac{t-t_1}{t_2}\right)\right) & \left(t_1 \le t \le t_d\right) \\ 0.74P_i^{0.17} + 2.71P_i^{0.28}.exp\left(-0.26P_i^{0.33}.\left(\dfrac{t-t_1}{t_2}\right)\right) & \left(t_d < t\right) \end{Bmatrix} \quad (7)$$

For $1 < P_i \le 100$ .

**Figure 1** (a) Idealised history of blast (Wu and Hao, 2005) and (b) Measured profile for 5 kg-TNT (Wu et al., 2021)

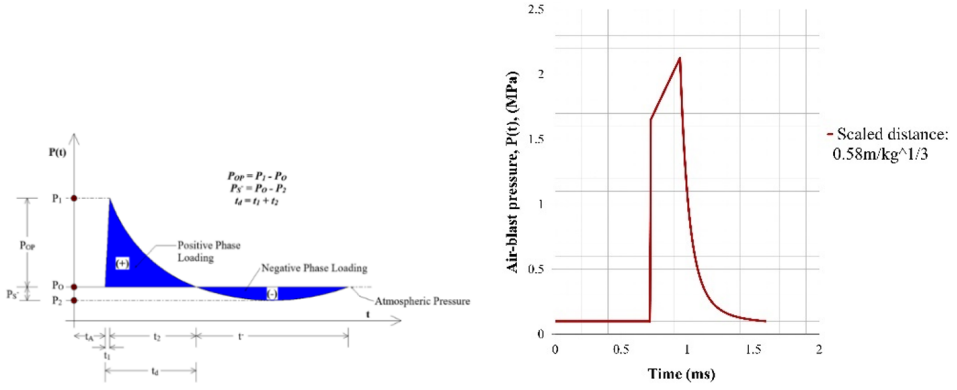


(a) (b)

TM5-1300 (1990), ASCE/SEI 59-11 (2011) and other blast design standards say that only positive pressure phase can be used for the assessment and planning of the concrete structure. The guidelines were created with the observation and findings of various studies and investigations in mind. These studies and investigations revealed that the value of the negative (suction) pressure phase is considerably less than atmospheric pressure, so it has no significant impact on the design of the structure (Ahmadi et al., 2021; Anas et al., 2020a, 2020b, 2020c; Anas et al., 2021a, 2021b; Anas and Alam, 2021a, 2021b; Anas et al., 2021c, 2021d, 2021e, 2021f; Anas and Alam, 2022a, 2022b, 2022c; Anas et al., 2022a, 2022b, 2022c, 2022d, 2022e, 2022f, 2022g, 2022h, 2022i, 2022j, 2022k; Ahmadi et al., 2022; Shariq et al., 2022a; 2022b, 2022c, 2022d; Tahzeeb

et al., 2022a, 2022b, 2022c; UlAin et al., 2021, 2022; Milani and Lourenco, 2009; Milani et al., 2009; Aamir et al., 2022; Anas et al., 2022l). It has also been thought that these values disregard the damage reactions. As a result, it is recommended to disregard the negative pressure phase when designing structures and only consider the positive phase, as shown in Figure 1.

### *4.2 Damage model*

A concrete damage model based on plasticity is known as the Concrete Damage Plasticity (CDP) Model. The model is used to design concrete and quasi-brittle materials that are taken into account in many sorts of structures, such as beams, columns, trusses, plates and solids (Ahmadi et al., 2021; Anas et al., 2020a, 2020b, 2020c; Anas et al., 2021a, 2021b; Anas and Alam, 2021a, 2021b; Anas et al., 2021c, 2021d, 2021e, 2021f; Anas and Alam, 2022a, 2022b, 2022c; Anas et al., 2022a, 2022b, 2022c, 2022d, 2022e, 2022f, 2022g, 2022h, 2022i, 2022j, 2022k; Ahmadi et al., 2022; Shariq et al., 2022a; 2022b, 2022c, 2022d; Tahzeeb et al., 2022a, 2022b, 2022c; UlAin et al., 2021, 2022; Milani and Lourenco, 2009; Milani et al., 2009; Aamir et al., 2022; Anas et al., 2022l). The model uses the isotropic damage elasticity concept (ABAQUS/CAE FEA Program, 2017; Hafezolghorani et al., 2017; Voyiadjis et al., 2008) and displays inelastic behaviour of concrete. The CDP model shows two different forms of concrete failures: compression crushing and tension cracking. The plasticity model may be used to depict these damages/cracks that are caused by the fracturing process in the model.

As seen in Figure 2, the damage plasticity is thought to be responsible for the concrete's uniaxial tensile and compressive response (ABAQUS/CAE FEA Program, 2017; Anas et al., 2020b; Voyiadjis et al., 2008). Up until the value of the failure stress reaches $\left(\sigma_{t0}\right)$, the stress-strain response under uniaxial tension displays a linear relationship. When this failure stress is exceeded, microcracks are created, which may be seen under a microscope using a stress-strain response (ABAQUS/CAE FEA Program, 2017; Anas and Alam, 2021b; Hafezolghorani et al., 2017). This strengthens the concrete structure's localisation of strain. The reaction in uniaxial compression stays linear until the initial yield value reaches $\left(\sigma_{C0}\right)$ (ABAQUS/CAE FEA Program, 2017; Voyiadjis et al., 2008). Stress handling in the plastic area, followed by strain softening above the ultimate stress $\left(\sigma_{cu}\right)$, serve as the primary indicators of response. Two hardening variables, $\epsilon_c^{pl,h}$ and $\epsilon_t^{pl,h}$, govern these failure surfaces. Uniaxial stress-strain curves are transformed into stress versus inelastic strain curves by ABAQUS/automated CAE's function (ABAQUS/CAE FEA Program, 2017; Hafezolghorani et al., 2017; Voyiadjis et al., 2008). Using statistical equations under compression and tensile loading in the CDP model, the uniaxial compression and tensile reactions of concrete are demonstrated. The following are the statistical formulae employed in the model:

$$\sigma_c = \left(1-d_c\right)E_0\left(\epsilon_c - \epsilon_c^{pl,h}\right) \tag{8}$$

Here, $\sigma_c$ = nominal compressive stress (MPa), $\sigma_{cu}$ = ultimate compressive stress (MPa), $\epsilon_c$ = compressive strain $\left(\epsilon_c^{pl,h} + \epsilon_c^{el}\right)$, $\epsilon_c^{pl,h}$ = compressive equivalent plastic strain, $\epsilon_c^{el}$ = elastic compressive strain.

$$\sigma_t = \left(1-d_t\right)E_0\left(\epsilon_t - \epsilon_t^{pl,h}\right) \tag{9}$$

Here, $\sigma_t$ = nominal tensile stress (MPa), $\sigma_{t0}$ = failure stress (MPa), $\epsilon_t$ = tensile strain $\left(\epsilon_t^{pl,h} + \epsilon_t^{el}\right)$, $\epsilon_t^{el}$ = elastic tensile strain. The model presupposes that a scalar degradation variable, "d", may be used to indicate how the material's modulus of elasticity has decreased.

$$E_a = \left(1 - d_{i=c,t}\right) E_0 \tag{10}$$

$E_u$ = reduced modulus of elasticity (MPa), $E_0$ = initial elasticity modulus of concrete (MPa), Damage parameters $d_c$ and $d_t$ range from zero to one (fully damaged material).

**Figure 2** Concrete reaction (ABAQUS/CAE FEA Program, 2017) under a uniaxial loading condition: (a) compression and (b) tension

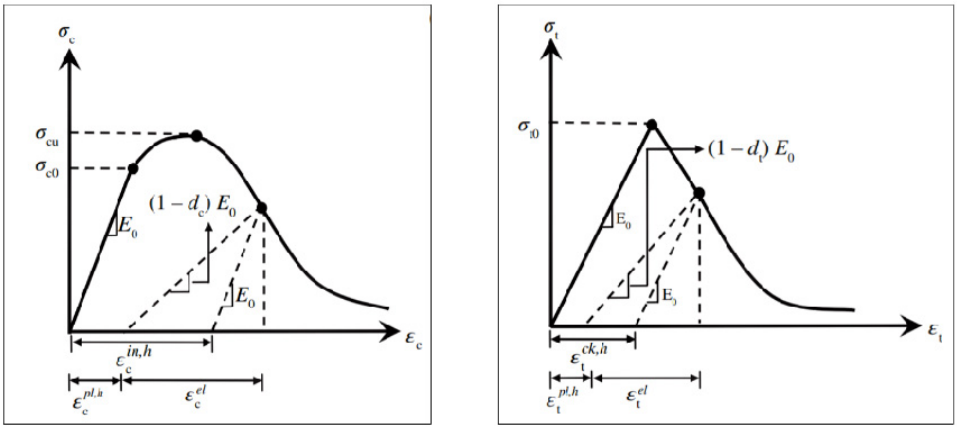


(a) (b)

## 5 Results and discussions

The 240 mm thick brick masonry wall's fracture pattern under the assumed TNT load is determined to be in excellent agreement with the experimental findings, as shown in Figure 3. The wall's maximum transverse displacement is 275.24 mm, Figures 4, 5 and 6 show that the related damage dissipation energy, compressive, tensile and shear stresses are 34400 J, 121.42 MPa, 0.02 MPa and 60.94 MPa. It is inferred that some of the bricks fall off the wall as observed in the trials from the estimated large transverse displacement (> wall thickness = 240 mm).

**Figure 3** Wall-US crack pattern comparison

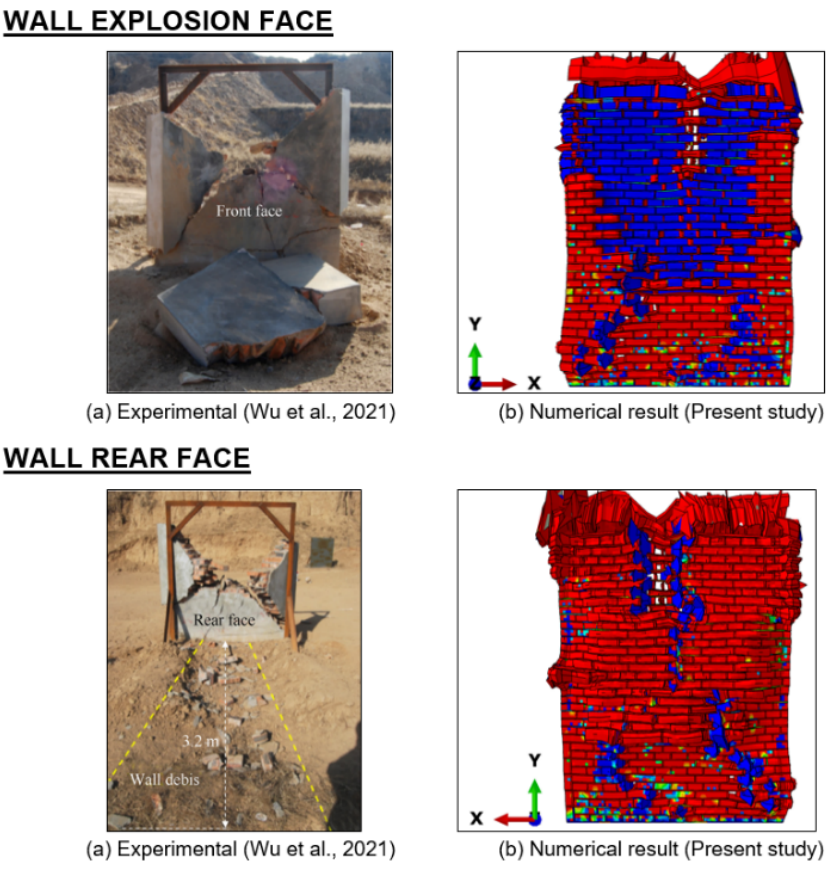


## *5.1 Response of wall strengthened with steel wire mesh on rear face only*

- According to calculations, the walls' maximum transverse displacements, designated as S-2.5-SWM-R, S-3.5-SWM-R and S-4.5-SWM-R, respectively, are 193.83 mm, 168.84 mm and 156.65mm, and their corresponding damage dissipation energies, indicated in Figure 4, are 19160 J, 18500 J and 17376 J.
- In comparison to the un-strengthened wall (US), Figure 6 shows that the compressive and shear stresses of the walls S-2.5-SWM-R, S-3.5-SWM-R and S-4.5-SWM-R are reduced by 83.48%, 86.83% and 86.04%, respectively, and by 83.30%, 89.46% and 91.79%, respectively. The brittle reaction of the wall is caused by higher tension reinforcing.
- When steel wire mesh with diameters of 2.5 mm, 3.5 mm and 4.5 mm is applied to a wall, the upper half of the mesh experiences tensile stresses of 250 MPa. However, according to Figure 7, the bottom half of the wire mesh's tensile stresses are 83.33 MPa and 41.67 MPa for horizontal wires with a diameter of 2.5 mm and 3.5 mm/4.5 mm, respectively.

The wall is strengthened with steel wire mesh reinforcement, which increases the wall's stiffness and integrity against blast loading (see Figure 5).

**Figure 4** Different FE models' transverse *Z*-displacement (mm)

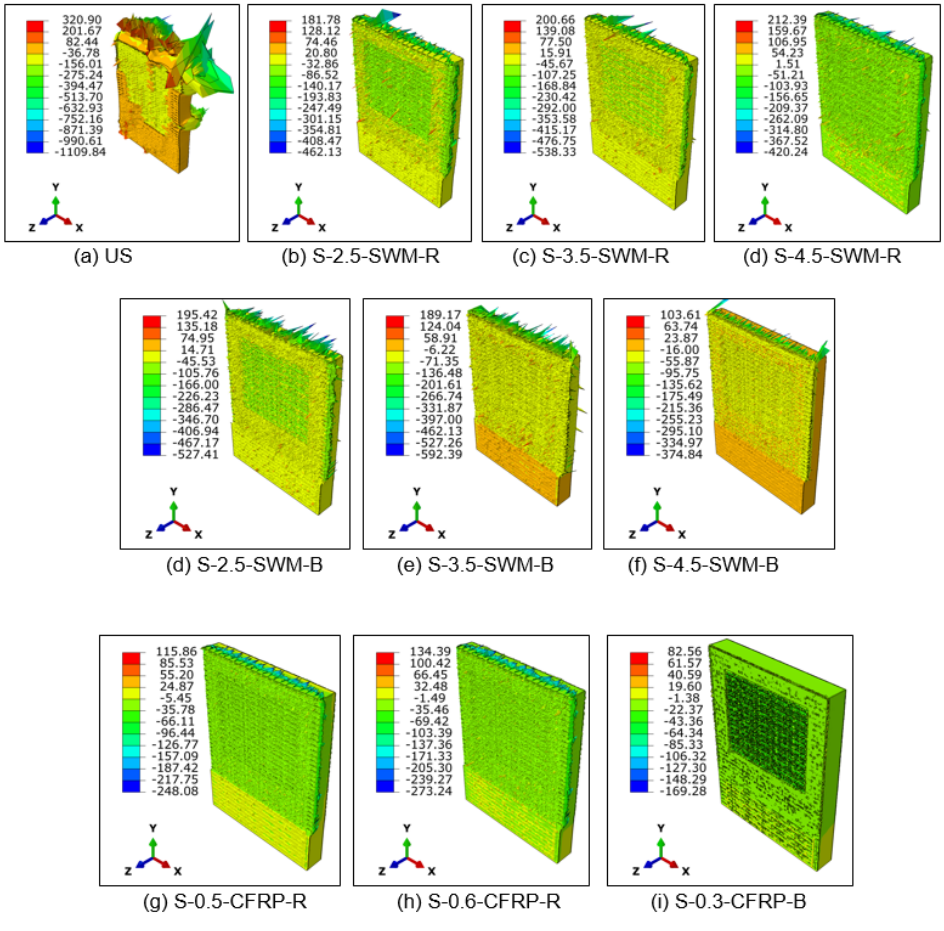

**Figure 5** Damage in different walls

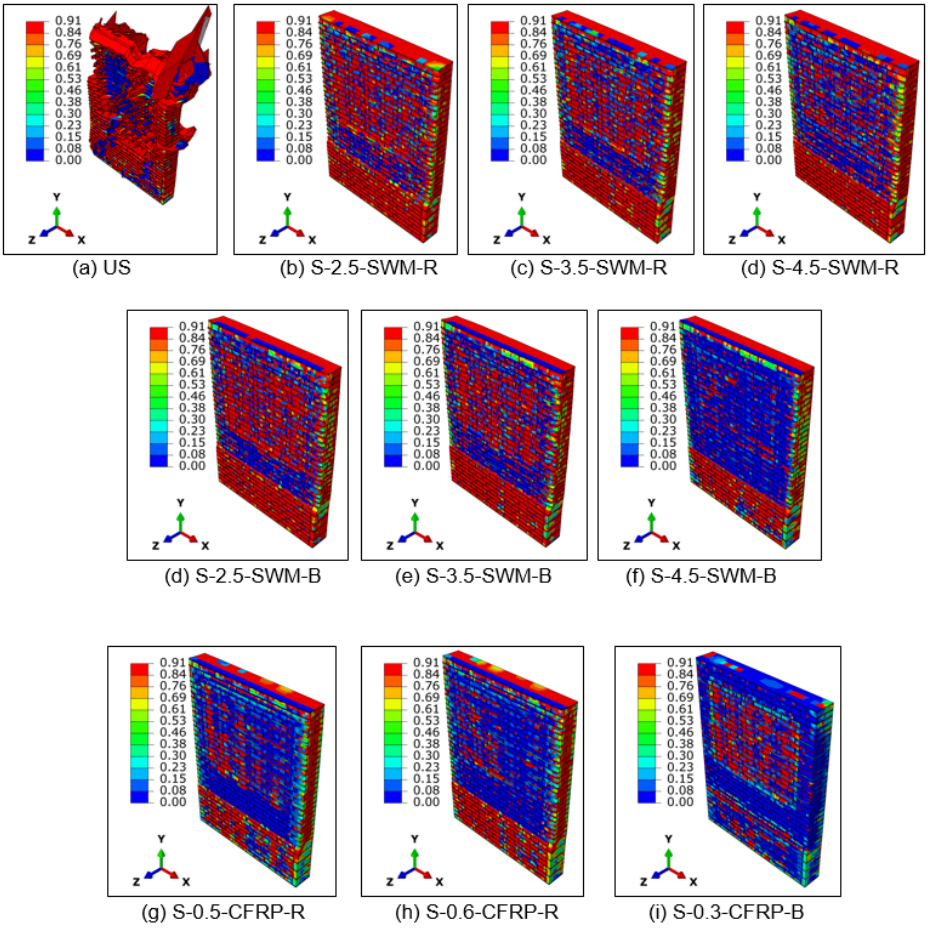


## *5.2 Response of wall strengthened with steel wire mesh on both faces*

- Walls S-2.5-SWM-B, S-3.5-SWM-B and S-4.5-SWM-B have steel wire mesh applied to both faces that reduces the maximum transverse displacement of the walls by 14.35%, 19.16% and 38.87%, respectively, in comparison to walls S-2.5-SWM-R, S-3.5-SWM-R and S-4.5-SWM-R, Figure 4.
- Compared to the walls S-2.5-SWM-R, S-3.5-SWM-R and S-4.5-SWM-R, the compressive and shear stresses of the S-2.5-SWM-B, S-3.5-SWM-B and S-4.5-SWM-B walls are reduced by 8.77%, 15.33% and 20.07%, respectively, and by 33.05%, 17.91% and –2.6%, respectively.

- According to Figure 7, the tensile stress on the top side of the back face of the wall with mesh on both faces is 208.33 MPa in 2.5 mm diameter. It decreases as the diameter rises, reaching 166.67 MPa in 3.5 mm and 125 MPa in 4.5 mm. The tensile stresses are shown to be lowering when the mesh is applied to both faces of the wall, as opposed to applying it to the wall's back face only.
- The brittle reaction of the reinforced wall is what is responsible for the increase in shear stress of the wall with 4.50 mm wire mesh on both faces.

**Figure 6** Principle stress distribution in bricks of several wall models under consideration

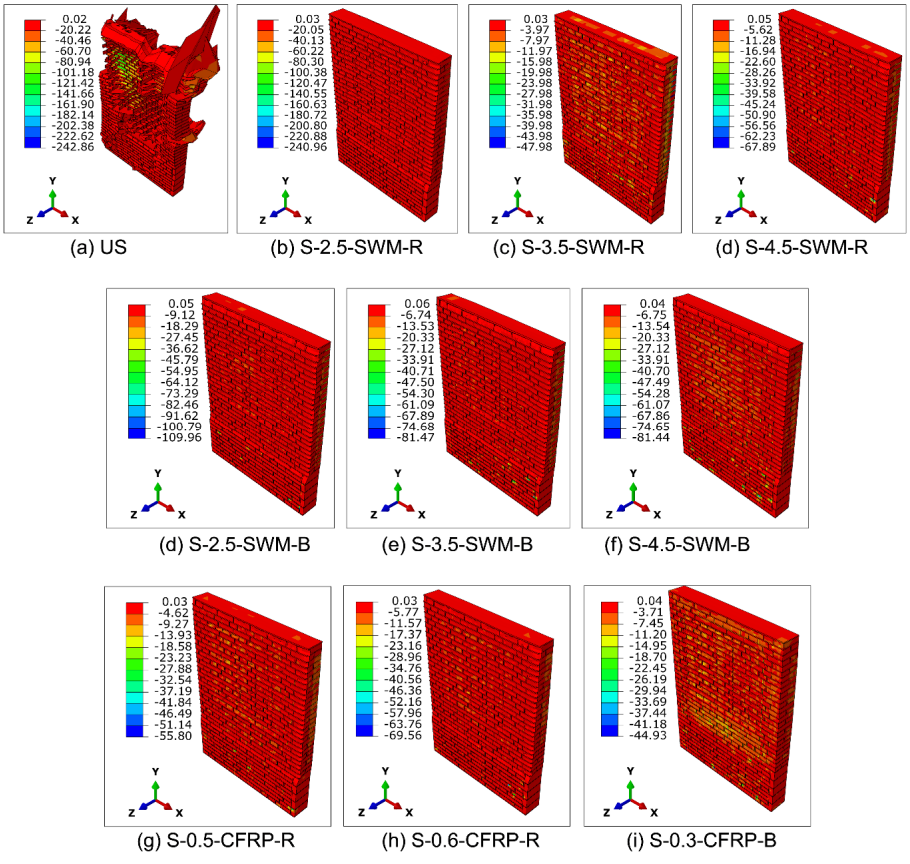

**Figure 7** Stress profiles of sheet and wrapping

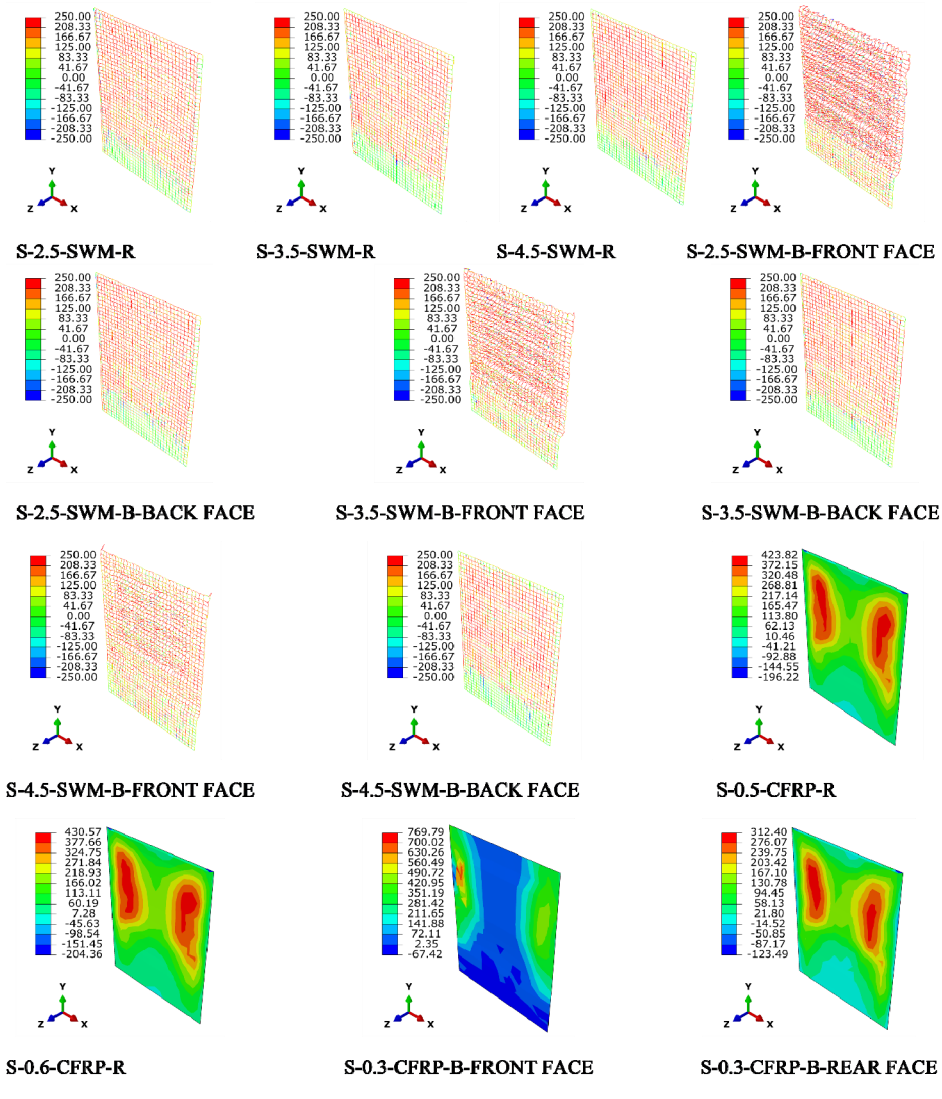


## *5.3 C-FRP strengthened masonry walls*

- When C-FRP is applied to the walls S-0.5-C-FRP-R, S-0.6-C-FRP-R and S-0.3-C-FRP-B, Figure 4 shows that the maximum transverse displacement is reduced by 64.96%, 74.77% and 76.62%, respectively, in comparison to the un-strengthened wall.
- Figure 4 shows that the wall with the 4.50 mm thick wire mesh sustains substantially less damage than the wall with the C-FRP, despite the maximum transverse displacement of the wall S-0.5-C-FRP-R being extremely similar to the displacement of the wall S-4.5-SWM-B (95.75 mm).

- The formation of extremely high in-plane stresses in the material of the sheet is what causes the enormous DDE of the reinforced wall made of C-FRP.

## 6 Conclusions

In the study, the following findings are drawn:

- Owing to the improper and inefficient brick layering during building of the wall and significant displacement, an unreinforced masonry wall sustains severe asymmetrical damage. The use of wire mesh on the back face not only prevents damage but also evenly distributes the intense masonry stresses throughout practically the whole wall. This causes the wall's displacement to decrease. Greater wire mesh diameter further reduces the masonry's stresses, resulting in less wall movement.
- The displacement is reduced when wire mesh is applied to the front face of a wall that already has mesh on the back face. In comparison to the 4.50 mm diameter mesh, the 2.50 and 3.50 mm diameter wire meshes on the front face of the wall are badly torn. The wire mesh on the front face can be thought of as sacrificial mesh since it dissipates energy.
- The C-FRP sheet on the wall's two faces is discovered to be a more efficient strengthening material to enhance the masonry wall's blast performance. The sheet may have served as a sacrifice layer to shield the wall from major damage and might have been changed out for a fresh one before it was exposed to more impulsive stresses.
- It is discovered that the wall responds comparably to the blast loading taken into account in this study when 4.50 mm wire mesh is applied to both faces and 0.50 mm C-FRP sheet is applied to the back face.

## References

Aamir, M., Alam, M. and Anas, S.M. (2022) 'Effect of blast location and explosive mass on the dynamic behavior of a bowstring steel highway girder bridge subjected to air-blast', *Materials Today: Proceedings*, Elsevier.

ABAQUS/CAE FEA Program (2017) *Concrete-Damaged Plasticity Model, Explicit Solver, Three-Dimensional Solid Element Library*, ABAQUS DS-SIMULIA User Manual.

Ahmadi, E., Alam, M. and Anas, S.M. (2021) 'Blast performance of RCC slab and influence of its design parameters', in Kolathayar, S., Ghosh, C., Adhikari, B.R., Pal, I. and Mondal, A. (Eds): *Resilient Infrastructure*, Springer, Singapore, pp.389-402. Doi: 10.1007/978-981-16-6978-1_31.

Ahmadi, E., Alam, M. and Anas, S.M. (2022) 'Behavior of C-FRP laminate strengthened masonry and unreinforced masonry compound walls under blast loading, Afghanistan scenario', *International Journal of Masonry Research and Innovation*.

Anas, S.M. and Alam, M. (2021a) 'Air-blast response of free-standing: (1) Unreinforced brick masonry wall, (2) Cavity RC wall, (3) RC walls with (i) Bricks, (ii) Sand, in the cavity: a macro-modeling approach', in Marano, G.C., Ray, C.S., UnniKartha, G., Kavitha, P.E., Prasad, R. and Achison, R.J. (Eds): *Proceedings of SECON'21*, Springer, Cham, pp.921–930. Doi: 10.1007/978-3-030-80312-4_78.

Anas, S.M. and Alam, M. (2021b) 'Comparison of existing empirical equations for blast peak positive overpressure from spherical free air and hemispherical surface bursts', *Iranian Journal of Science Technology, Transactions of Civil Engineering*, Vol. 46, pp.965–984. Doi: 10.1007/s40996-021-00718-4.

Anas, S.M. and Alam, M. (2022a) 'Performance of simply supported concrete beams reinforced with high-strength polymerre-bars under blast-induced impulsive loading', *International Journal of Structural Engineering*, Vol. 12, No. 1, pp.62–76. Doi: 10.1504/IJSTRUCTE.2022.119289.

Anas, S.M. and Alam, M. (2022b) 'Performance of brick-filled reinforced concrete composite wall strengthened with C-FRP laminate(s) under blast loading', *Materials Today: Proceedings*, Elsevier. Doi: 10.1016/j.matpr.2022.03.162.

Anas, S.M. and Alam, M. (2022c) 'Role of shear reinforcements on the punching shear resistance of two-way RC slab subjected to impact loading', *Materials Today: Proceedings*, Elsevier.

Anas, S.M., Alam, M. and Shariq, M. (2022e) 'Damage Response of Conventionally Reinforced Two-way Spanning Concrete Slab under Eccentric Impacting Drop Weight Loading', *Defence Technology*. Doi: 10.1016/j.dt.2022.04.011.

Anas, S.M., Alam, M. and Shariq, M. (2022h) 'Behavior of two-way RC slab with different reinforcement orientation layouts of tension steel under drop load impact', *Materials Today: Proceedings*, Elsevier.

Anas, S.M., Alam, M. and Tahzeeb, R. (2022j) 'Impact response prediction of square RC slab of normal strength concrete strengthened with (1) laminates of (i) mild-steel and (ii) C-FRP, and (2) strips of C-FRP under falling-weight load', *Materials Today: Proceedings*, Elsevier. Doi: 10.1016/j.matpr.2022.07.324.

Anas, S.M., Alam, M. and Umair, M. (2020a) 'Performance of one-way concrete slabs reinforced with conventional and polymer re-bars under air-blast loading', in Chandrasekaran, S., Kumar, S. and Madhuri, S. (Eds): *Recent Advances in Structural Engineering*, Vol. 135, pp.179–191. Doi: 10.1007/978-981-33-6389-2_18.

Anas, S.M., Alam, M. and Umair, M. (2020b) 'Performance of one-way composite reinforced concrete slabs under explosive-induced blast loading', *IOP Conference Series: Earth and Environmental Science*, Tashkent, Uzbekistan. Doi: 10.1088/1755-1315/614/1/012094.

Anas, S.M., Alam, M. and Umair, M. (2021b) 'Experimental and numerical investigations on performance of reinforced concrete slabs under explosive-induced air-blast loading: a state-of-the-art review', *Structures*, Elsevier, Vol. 31, pp.428–461. Doi: 10.1016/j.istruc.2021.01.102.

Anas, S.M., Alam, M. and Umair, M. (2021c) 'Performance of on-ground double-roof RCC shelter with energy absorption layers under close-in air-blast loading', *Asian Journal of Civil Engineering*, Vol. 22, pp.1525–1549. Doi: 10.1007/s42107-021-00395-8.

Anas, S.M., Alam, M. and Umair, M. (2021d) 'Air-blast and ground shockwave parameters, shallow underground blasting, on the ground and buried shallow underground blast-resistant shelters: a review', *International Journal of Protective Structures*, Vol. 13, No. 1, pp.99–139. Doi: 10.1177/2F20414196211048910.

Anas, S.M., Alam, M. and Umair, M. (2021e) 'Out-of-plane response of clay brick unreinforced and strengthened masonry walls under explosive-induced air-blast loading', in Kolathayar, S., Ghosh, C., Adhikari, B.R., Pal, I. and Mondal, A. (Eds): *Resilient Infrastructure*, Springer, Singapore, pp.477–491. Doi: 10.1007/978-981-16-6978-1_37.

Anas, S.M., Alam, M. and Umair, M. (2021f) 'Influence of charge locations on close-in air-blast response of pre-tensioned concrete U-girder', in: Kolathayar, S., Ghosh, C., Adhikari, B.R., Pal, I. and Mondal, A. (Eds): *Resilient Infrastructure*, Springer, Singapore, pp.513–527. Doi: 10.1007/978-981-16-6978-1_40.

Anas, S.M., Alam, M. and Umair, M. (2022b) 'Strengthening of braced unreinforced brick masonry wall with (i) C-FRP wrapping, and (ii) Steel angle-strip system under blast loading', *Materials Today: Proceedings,* Elsevier. Doi: 10.1016/j.matpr.2022.01.335.

Anas, S.M., Alam, M. and Umair, M. (2022c) 'Effect of design strength parameters of conventional two-way singly reinforced concrete slab under concentric impact loading', *Materials Today: Proceedings,* Elsevier. Doi: 10.1016/j.matpr.2022.02.441.

Anas, S.M., Alam, M. and Umair, M. (2022d) 'Performance based strengthening with concrete protective coatings on braced unreinforced masonry wall subjected to close-in explosion', *Materials Today: Proceedings,* Elsevier, https://doi.org/10.1016/j.matpr.2022.04.206.

Anas, S.M., Alam, M. and Umair, M. (2022g) 'Performance of (1) concrete-filled double-skin steel tube with and without core concrete, and (2) concrete-filled steel tubular axially loaded composite columns under close-in blast', *International Journal of Protective Structures*. Doi: 10.1177/2F20414196221104143.

Anas, S.M., Alam, M. and Umair, M. (2022i) 'Air-blast response of axially loaded clay brick masonry walls with and without reinforced concrete core', in Fonseca de Oliveira Correia, J.A. et al. (Eds.): *Advances in Structural Mechanics and Applications*, pp.1–18. Doi: 10.1007/978-3-030-98335-2_4.

Anas, S.M., Alam, M. and Umair, M. (2022k) 'Experimental studies on blast performance of unreinforced masonry (URM) walls of clay bricks and concrete blocks: a state-of-the-art review', *International Journal of Masonry Research and Innovation*.

Anas, S.M., Alam, M. and Umair, M. (2022l) 'Performance prediction of braced unreinforced and strengthened clay brick masonry walls under close-range explosion through numerical modeling', *International Journal of Computational Materials Science and Surface Engineering*.

Anas, S.M., Ansari, M.I. and Alam, M. (2020c) 'Performance of masonry heritage building under air-blast pressure without and with ground shock', *Australian Journal of Structural Engineering*, Vol. 21, No. 4, pp.329–344. Doi: 10.1080/13287982.2020.1842581.

Anas, S.M., Ansari, M.I. and Alam, M. (2021a) 'A study on existing masonry heritage building to explosive-induced blast loading and its response', *International Journal of Structural Engineering*, Vol. 11, No. 4, pp.387–412. Doi: 10.1504/IJSTRUCTE.2021.118065.

Anas, S.M., Shariq, M. and Alam, M. (2022a) 'Performance of axially loaded square RC columns with single/double confinement layer(s) and strengthened with C-FRP wrapping under close-in blast', *Materials Today: Proceedings*, Elsevier. Doi: 10.1016/j.matpr.2022.01.275.

Anas, S.M., Shariq, M., Alam, M. and Umair, M. (2022f) 'Evaluation of critical damage location of contact blast on conventionally reinforced one-way square concrete slab applying CEL-FEM blast modeling technique', *International Journal of Protective Structures*. Doi: 10.1177/2F20414196221095251.

ASCE/SEI 59-11 (2011) 'Blast protection of buildings', *American Society of Civil Engineers*, U.S.

Badshah, E., Naseer, A., Ashraf, M. and Ahmad, T. (2021) 'Response of masonry systems against blast loading', *Defence Technology*, Vol. 17, pp.1326–1337.

Ehsani, M. and Pena, C. (2009) 'Blast loading Retrofit of unrein forced masonry walls', *Structural Magazine*, pp.16–20.

Goel, D.M. and Matsagar, A.V. (2014) 'Blast-resistant design of structures', *Practice Periodical on Structural Design and Construction*, ASCE, Vol. 19, No. 2, pp.1–9.

Hafezolghorani, M., Hejazi, F., Vaghei, R., Saleh, M. and Karimzade, K. (2017) 'Simplified damage plasticity model for concrete', *Structural Engineering International*, pp.68–78.

Hao, H., Hao, Y., Li, J. and Chen, W. (2016) 'Review of the current practices in blast resistant analysis and design of concrete structures', *Advances in Structural Engineering*, Vol. 19, No. 8, pp.1193–1223.

IS 4948 (2002) *Welded Steel Wire Fabric for General Use*, Bureau of Indian Standards, New Delhi, India.

IS 4991 (1968) *Criteria for Blast Resistant Design of Structures for Explosions above Ground*, Bureau of Indian Standard, New Delhi, India.

Milani, G. and Lourenco, P.B. (2009) 'Blast analysis of enclosure masonry walls using homogenization approaches', *Multiscale Computational Engineering*, Vol. 7, No. 2, pp.91–113.

Milani, G., Lourenco, P.B. and Tralli, A. (2009) 'Homogenized rigid: plastic model for masonry walls subjected to impact', *International Journal of Solids and Structures*, Vol. 46, pp.4133–4149.

Myers, J.J., Belarbi, A. and Domiaty, K.A. (2004) 'Blast resistance of FRP retrofitted un-reinforced masonry (URM) walls with and without arching action', *TMS Journal*, pp.9–26.

Pandey, A.K. and Bisht, R.S. (2014) 'Numerical modelling of infilled clay bricks masonry under blast loading', *Advances in Structural Engineering*, Vol. 17, No. 4, pp.591–606.

Phan-Vu, P., Tran, D.T., Pham, T.M., Dang, T.D., Ngo-Huu, C. and Nguyen-Minh, L. (2021) 'Distinguished bond behaviour of C-FRP sheets in unbonded post-tensioned rein-forced concrete beams versus single-lap shear tests', *Engineering Structures*, Elsevier, Vol. 234. Doi: 10.1016/j.engstruct.2020.111794.

Shamim, S., Ahmad, S. and Khan, A.K. (2019). Finite element analysis of masonry wall subjected to blast loading', *International Journal of Advances in Mechanical and Civil Engineering*, pp.40–43.

Shariq, M., Alam, M. and Husain, A. (2022d) 'Performance of RCC column retrofitted with C-FRP wrappings and the wrappings with steel angle-batten jacketing under blast loading', in Nandagiri, L., Narasimhan, M.C. and Marathe, S. (Eds): *Recent Advances in Civil Engineering*, Springer, Singapore. Doi: 10.1007/978-981-19-1862-9_21.

Shariq, M., Alam, M., Husain, A. and Anas, S.M. (2022a) 'Jacketing with steel angle sections and wide battens of RC column and its influence on blast performance', *Asian Journal of Civil Engineering*, Springer. Doi: 10.1007/s42107-022-00437-9.

Shariq, M., Alam, M., Husain, A. and Islam, N. (2022c) 'Response of strengthened unreinforced brick masonry wall with (1) mild steel wire mesh and (2) C-FRP wrapping, under close-in blast', *Materials Today: Proceedings*, Elsevier. Doi: 10.1016/j.matpr.2022.05.153.

Shariq, M., Saifi, F., Alam, M. and Anas, S.M. (2022b) 'Effect of concrete strength on the dynamic behavior of axially loaded reinforced concrete column subjected to close-range explosive loading', *Materials Today: Proceedings*, Elsevier. Doi: 10.1016/j.matpr.2022.07.313.

Tahzeeb, R., Alam, M. and Mudassir, S.M. (2022a) 'A comparative performance of columns: reinforced concrete, composite, and composite with partial C-FRP wrapping under contact blast', *Materials Today: Proceedings*, Elsevier. Doi: 10.1016/j.matpr.2022.03.367.

Tahzeeb, R., Alam, M. and Mudassir, S.M. (2022b) 'Performance of composite and tubular columns under close-in blast loading: a comparative numerical study', *Materials Today: Proceedings*, Elsevier. Doi: 10.1016/j.matpr.2022.04.587.

Tahzeeb, R., Alam, M. and Mudassir, S.M. (2022c) 'Effect of transverse circular and helical reinforcements on the performance of circular RC column under high explosive loading', *Materials Today: Proceedings*, Elsevier. Doi: 10.1016/j.matpr.2022.04.676.

TM 5-1300 (1990) *Structures to Resist the Effect of Accidental Explosions*, Technical Manual, Joint Department of the Army, the Navy, and the Air Force, US.

UlAin, Q., Alam, M. and Anas, S.M. (2021) 'Behavior of ordinary load-bearing masonry structure under distant large explosion, Beirut scenario', in Kolathayar, S., Ghosh, C., Adhikari, B.R., Pal, I. and Mondal, A. (Eds): *Resilient Infrastructure*, Springer, Singapore, pp.239–253. Doi: 10.1007/978-981-16-6978-1_19.

UlAin, Q., Alam, M. and Anas, S.M. (2022) 'Response of two-way RCC slab with unconventionally placed reinforcements under contact blast loading', in Fonseca de Oliveira Correia, J.A. et al. (Eds.): *Advances in Structural Mechanics and Applications*, pp.1–18. Doi: 10.1007/978-3-031-04793-0_17.

Voyiadjis, G.Z., Taqieddin, Z.N., Kattan, P.I. (2008) 'Anisotropic damage-plasticity model for concrete', *International Journal of Plasticity*, Vol. 24, pp.1946–1965.

Wei, J., Du, Z., Zheng, Y., Ounhueane, O. (2021) 'Research on damage characteristics of bricks masonry under explosion load', *Shock and Vibration*.

Wei, X. and Strewart, M.G. (2010) 'Model validation and parametric study on the blast response of unreinforced brick masonry walls', *International Journal of Impact Engineering*, Vol. 37, pp.1150–1159.

Wu, C. and Hao, H. (2005) 'Modelling of Simultaneous ground shock and air blast pressure on nearby structures from surface explosions', *International Journal of Impact Engineering*, Vol. 31, pp.699–717.

Wu, G., Ji, C., Wang, X., Gao, F., Zhao, C., Liu, Y. and Yang, G. (2021) 'Blast response of clay brick masonry unit walls unreinforced and reinforced with polyurea elastomer', *Defence Technology*, Vol. 18, No. 4, pp.643–662.